Available online at www.sciencedirect.com
SCIENCE DIRECT®
Talanta 65 (2005) 1286–1294
Talanta
www.elsevier.com/locate/talanta

Laser-induced particulate as carrier of analytical information in LA-ICPMS direct solid microanalysis

Davide Bleiner*, Peter Lienemann, Heinz Vonmont

EMPA-Swiss Federal Laboratories for Materials Testing and Research, Überlandstrasse 129, CH 8600 Dübendorf, Switzerland

Received 15 April 2004; received in revised form 7 September 2004; accepted 9 September 2004
Available online 12 October 2004

Abstract

Laser ablation in combination with plasma spectrochemistry is an ideal technique for depth profiling analysis, based on signal profiles. However, signal profiles were found to be critically influenced by the characteristics of the ablated particles, especially their composition and size distribution, and consequently transport mechanism and plasma-assisted vaporization efficiency. Even for a refractory material like ceramic, relics of melting following laser irradiation were found, so that particles were non-stoichiometric as compared to the parent material. Estimates of transport efficiency showed that this is highly variable as a function of particle size. Large particles are likely to be lost in the sample chamber. Fine particles are prone to wall reaction, especially in Ar ambient. Variability in particle delivery to the ICP-MS was suspected to be the cause for an element-dependent analyte signal response. Fluctuation in particle vaporization degree as a consequence of plasma temperature instability was also responsible for element-dependent signal profile deviation. However, for a 10-fold higher mass load into the plasma, no direct fractionation effects were observed. Differential transport of chemically-differentiated analyte-carriers is suggested to be primary cause for element-dependent signal structure.

Keywords: Laser ablation inductively coupled plasma; Aerosol; Fractionation; Wall reaction; Ablation set-up; Signal profile

1. Introduction

The use of laser beams combined to plasma spectrochemistry for direct solid sample analysis or for depth profiling has become more and more popular in several applicative fields (e.g. geosciences, forensic, materials), due to versatility, detection power, and dynamic range of the technique [1]. Concerning the sampling stage, different wavelengths [2–5], laser pulse widths [6,7], and beam energy profiles [8] have been investigated, so that our current understanding of laser-assisted micro-sampling bases upon solid foundations. Nevertheless, the issue of quantification is still not completely matched for all kind of possible applications, for which LA-ICPMS represents an ideal tool.

Several authors [9–24] have reported inconsistent time-dependent signal response during laser ablation of certain matrices (so-called 'fractionation'), leading to improper quantification. Different presumable sources of fractionation have been investigated, like laser-induced solid modification [16,19], fractional particle transport [12,18,19], incongruent particle atomization in the ICP [10,24], though none of them was found to be 'the big one'.

Fractionation limits quantification capability if quantitation is performed in depth-resolved mode, because when calibration factors fluctuate during the acquisition of element concentration profiles, one might not be able to extract real composition profiles. Therefore, depth profile analysis is the most suffering analytical application for fractionation effects, because it depends on signal profile characteristics, not simply the integrals.

Signal profile characteristics are influenced by each stage of LA-ICPMS measurements, i.e. beam delivery, particle

* Corresponding author. Tel.: +41 1 823 4602; fax: +41 1 821 6244.
E-mail address: davide.bleiner@empa.ch (D. Bleiner).

0039-9140/$ – see front matter © 2004 Elsevier B.V. All rights reserved.
doi:10.1016/j.talanta.2004.09.004

ablation, particle transport, particle atomization, ionization, ion-extraction, and ion-detection. Primary importance have the laser-induced particles, e.g. whether these particles are representative of the parent material composition (stoichiometric sampling), whether they are transported efficiently and steadily along the tube (non-fractionated transport), whether these particles are responsible for significant instabilities in the ICP, which affect particle atomization mechanism and signal response.

Aim of the present paper is to investigate the implications of particle-related processes on LA-ICPMS signal profiles. Particle characteristics were examined and related to analytical signal characteristics. Sample delivery for different size classes was estimated and wall reaction was described on theoretical basis. Sample delivery fluctuation was compared to variations of sample atomization/ionization efficiency in the ICP, to define the most significant source of signal profile deviation. Considerations on signal structure and analytical capabilities will be given throughout.

2. Experimental

2.1. Samples

$La_{0.7}Sr_{0.3}MnO_3$ ceramic powders (perovskite) were separated into size fractions by means of a cyclone air-separator (Alpine AG, Germany) at seven different angular velocities (2000 to 10,000 rpm) that corresponded to particle sizes in the range 1–20 μm, and with sieves for the larger fractions up to 180 μm. A batch of size-classed powders was obtained and the size distribution of the used ones is shown in Fig. 1. Fraction four extends more widely than the others into the fine grained region. Size distributions were measured using an optical particle size measurement device (Malvern Mastersizer X). Multi-elemental analyses using ICP-MS were done after digestion with 15 mL of $HCl + HNO_3$ 2:1 at approximately 100 °C, and identical results for all size fractions of the raw powders were obtained, shown in Table 1. Pressed pellets were prepared using 1 mL of cellulose 1% aqueous solution as binder. For every pellet 10 g of raw powder were used and pressed at 300 kg/cm^2. The pellets were dried at 80 °C in oven (Hereaus GmbH, Germany). A blank was prepared with cellulose powder for quality control.

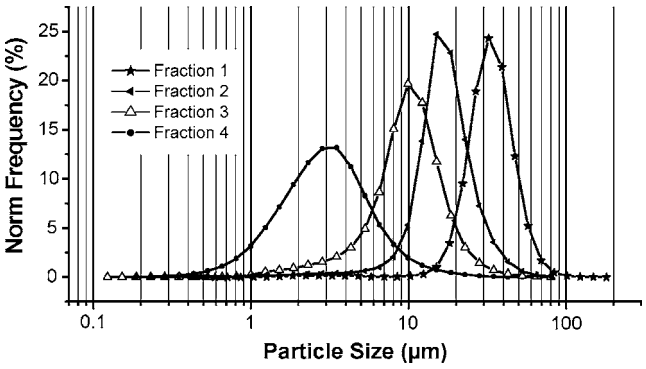

Fig. 1. Particle size distribution for the analysed classed fractions.

Table 1
Composition of the analysed samples as revealed by ICP-MS analysis

Element	Concentration
La (%)	52.6
Mn (%)	27.8
Sr (%)	8.7
Co (mg/kg)	373
Y (mg/kg)	24
Zr (mg/kg)	21

Oxygen is further matrix element. Measurement uncertainty was about 1% R.S.D.

2.2. Instrumentation

A commercially available PE 320 Nd:YAG was in-house modified [25–27]. Frequency-quadrupled wavelength (266 nm) was generated with two HG-crystals, and with a set of five dichroic plates (Melles Griot GmbH, Germany), wavelength selection was operated. The laser was operated at 10 pulses per second, with pulse energy of 4 mJ resulting in a fluence of 50 J/cm^2. The beam power was let stabilize for 20 min and then the laser was left in run mode during the whole measurement period, using a shutter for preventing the beam from reaching the sample when the case. The laser beam was focused with a $f = 40$ mm plano-convex lens. A pinhole was used to control the spot size, by imaging it onto the sample surface. The ablation cell was 1.4 cm^3 own design, with a 0.5 mm i.d. inlet nozzle to ensure a steady gas jet. The transport tube was a 4 mm i.d. and 1.5 m long PVC tube. Argon was used as carrier gas at a flow of 0.9 L/min. The ICP-MS was a quadrupole plasma-mass spectrometer (PE/Sciex Elan 6000) operated under standard conditions. A menu of six elements was edited with a dwell time of 20 ms. Background signal was monitored at mass 220.5 (off-peak) and for 20 s previous the operation of the laser on the analytes mass (on-peak). SEM-EDX measurements were performed using a field emission Jeol JSM-6300F instrument, with accelerating voltage in the range 0.5–30 kV, and capabilities to detect from boron to uranium with a 140 eV peak resolution. The imaging allows magnification in the range 10X–500,000X with optimum resolution of 1.5 nm.

2.3. Data collection and processing

LA-ICPMS data were acquired after surfaces were previously ablated with about 20 pulses, which permitted to eliminate a large signal spike at the onset of the ablation (Fig. 2). The data were recalculated using own written spreadsheet macro (Elektra). Data reduction implied background subtraction (on-peak), signal integration, noise determination as 1 s, mean values calculation from $n = 7$ replicates. Particles falling off onto the sample surface during the ablation

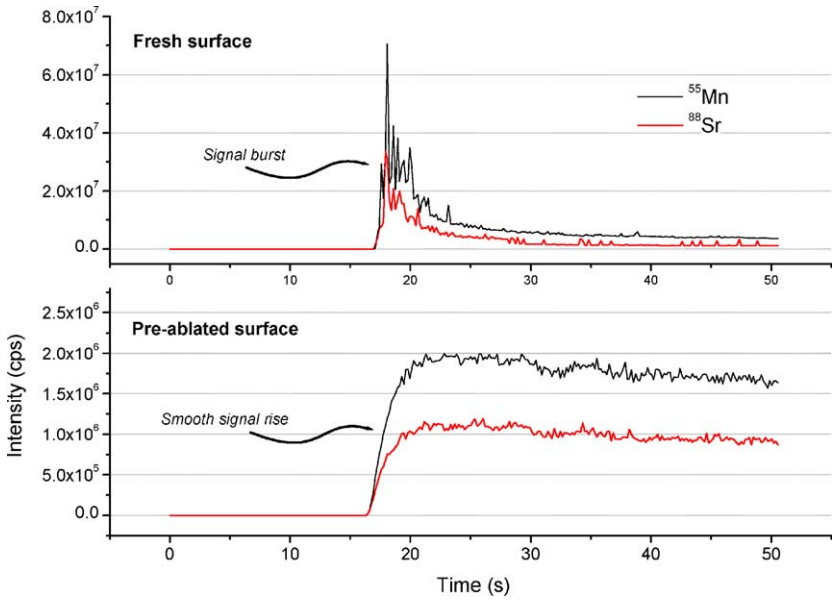

Fig. 2. Signal profile without and with surface pre-ablation.

experiments were analysed using SEM-EDX, shortly after ablation experiments. Different sample portions were investigated taking care to avoid grain edges to be sure that the electron probe would measure representatively. Reproducibility of SEM-EDX analyses was <2% R.S.D.

3. Results and discussion

3.1. Particles characteristics and signal profile

Laser ablation experiments using 266 nm led to the formation of different particles, whose characteristics influenced signal structure. The extent of the interrelation among particulate characteristics and signal profile was investigated using pressed pellets of classed grain size. Laser ablation of size-classed pellets permitted a control over particle introduction into the ICP in a size-dependent way. This situation represented a benchmark for the investigation of particle-related effects in LA-ICPMS determinations. In a first instance, the ablated particles were carefully investigated to assess compositional characteristics. Fig. 3 shows SEM images of several ablation products. The fall-out particles were found to decrease in size as a function of distance from the crater rim, the coarser next to the crater. Fig. 3(A) and 3(B) show particles deposited next to the crater edge, and at about 80–100 μm away of it, respectively. Fig. 3(C) and 3(D) show large particles produced by aggregation of fragments, which however, did occur farther on the sample surface than what shown in Fig. 3(B). Individual particles ($n = 20$) were analysed by SEM-EDX and found to be chemically heterogeneous (Fig. 4). Oxygen signal demonstrates that compositional variability is not due to instrumental drift. ICP-MS analyses were used as reference composition to define the extent of composition deviation due to laser irradiation. Results indicated that even using UV radiation chemical differentiation still characterizes the ablation products, which matches with what already reported elsewhere for IR radiation [18,19]. Large portions of melting were identified also from this refractory sample like the analysed ceramic. The occurrence of thermal effects is supposed to be the cause for particle chemical heterogeneity. With respect to this, incomplete particle delivery or atomization/ionization becomes critical for the overall analytical performance. Signal profiles of variable intensity and stability were obtained and Fig. 5 shows signal structure as a function of particle size for Sr. This figure clearly shows that fine fractions delivery is more turbulent that larger fractions, being the former more sensitive to gas phase flow regime. Fine fraction transport efficiency was experimentally found to be higher as indicated by the integrals, though noisier as said above. Then, fine fractions were better suspended into the flowing carrier gas than the bulkier counterparts.

3.2. Sample delivery

The entrainment and transport of particles along the set-up is such a critical aspect to determine signal profile. Particles are carrier of the analytical information. Particles were found to be chemically heterogeneous. Then, if transport efficiency is a function of particle size, LA-ICPMS signals can behave very different for individual elements depending on ‘what element in what particle size’. Therefore, estimates of particle size-dependent transport efficiency were done. An estimate of the relative transport efficiency was possible from the signal intensity obtained after ablation of size-classed samples,

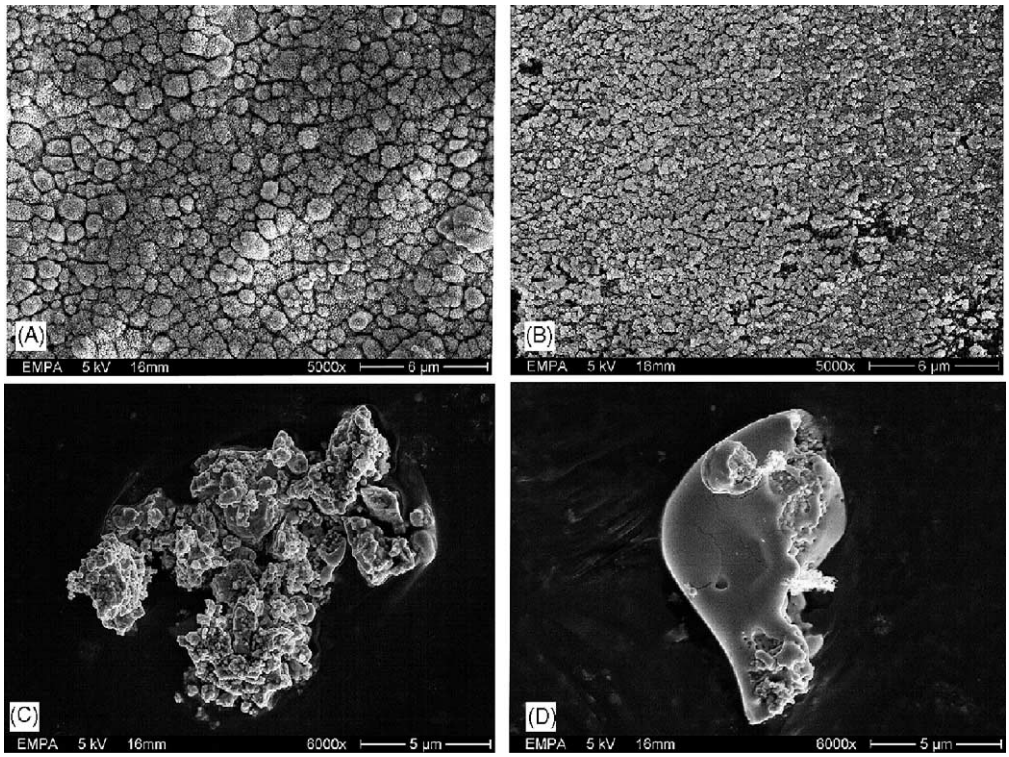

Fig. 3. SEM images of ablation products. (A) Debris next to the ablation pit; (B) debris away from the ablation pit; (C) aggregated clump produced by connection of molten particles and fragments; (D) particle that has experienced extensive melting.

using the following relation:

$$N \propto \frac{I_{\text{net}}}{R^3}$$

where N is the number of particles transported, I_{net} is net signal intensity and R is particle radius (assumed spherical). The equation is fully explained in the Appendix. Fig. 6 shows the obtained transport efficiencies for all particle fractions investigated. Transport efficiency was found to be largely dependent on particle size, varying from below the percent for coarse particles up to 98% for the finer fractions. It should be pointed out that this estimate refers to the number of particles, whereas the signal intensities shown in Fig. 5 give indications of the transport efficiency based on mass. Since mass is a cubic function of size (at constant density), this almost two-orders of magnitude difference in particle number transport efficiency would indicate a factor of four higher signal intensity for fine versus large particles. In the estimate done, it was assumed that particle vaporization degree is uniform for all the investigated fractions, which seemed a reasonable

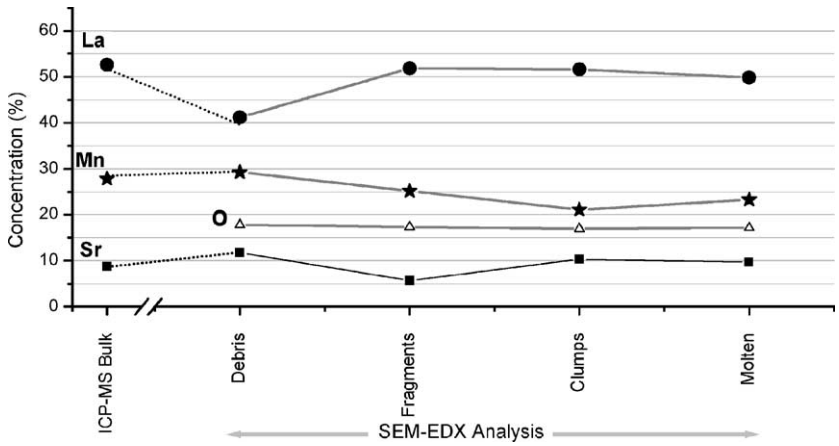

Fig. 4. SEM-EDX measurements on different ablation products and ICP-MS analysis.

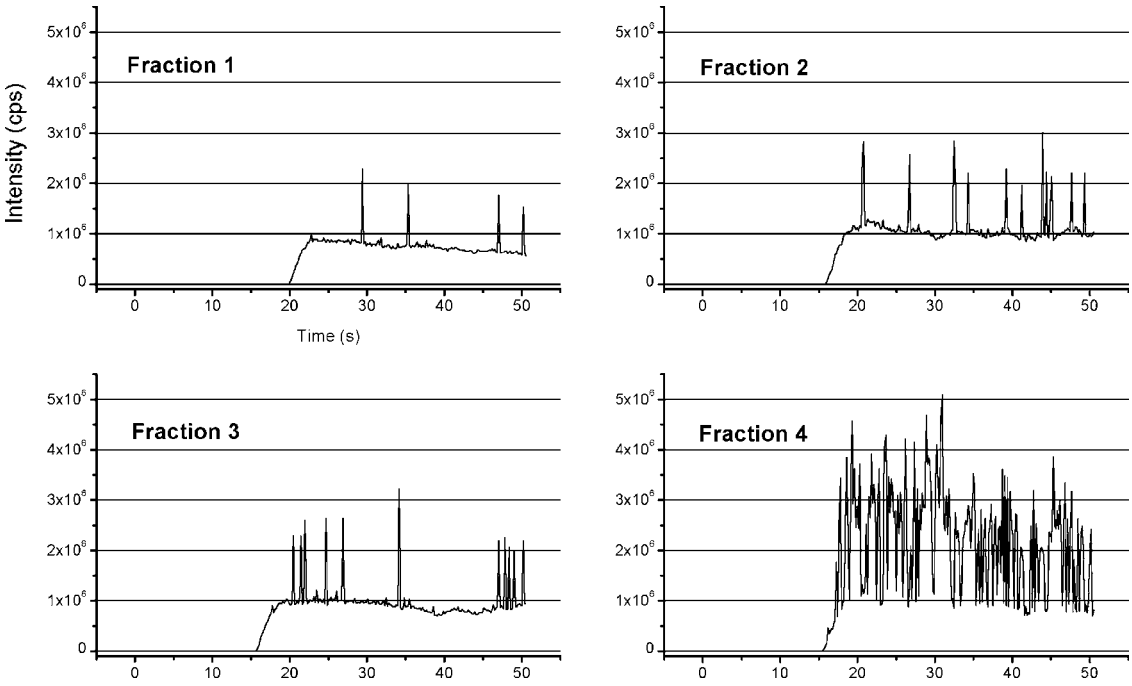

Fig. 5. LA-ICPMS signal profiles for different particle size fractions, as given in Fig. 1.

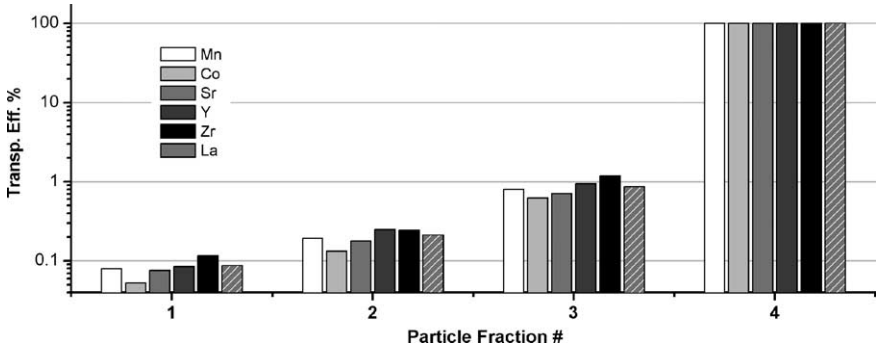

Fig. 6. Estimated transport efficiency for different particle size fractions, as given in Fig. 1.

assumption for only micro-sized particulate. Transient deviations from this assumption might explain differences in signal intensity. In any case, for nano-sized particles vaporization degree is surely different and presumably higher, which did not allow exporting the conclusions to such fractions in the same measurement. Fine particles were also prone to clump which rendered the determination cumbersome and less reliable.

The results discussed so far would indicate that elements that enrich in fine particles are more efficiently transported. However, fine particles are more sensitive to ambient gas characteristics due to higher diffusion coefficient and wall

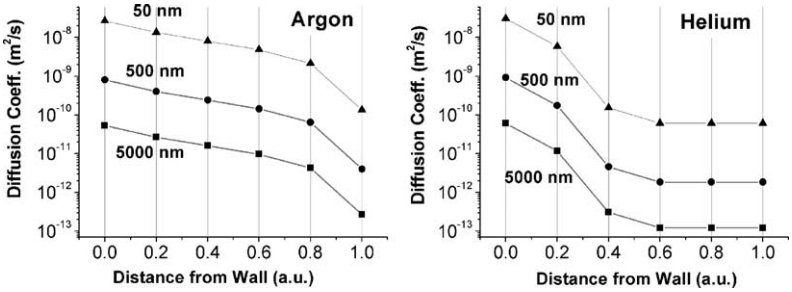

Fig. 7. Calculated diffusion coefficient for argon and helium and values for different particle sizes.

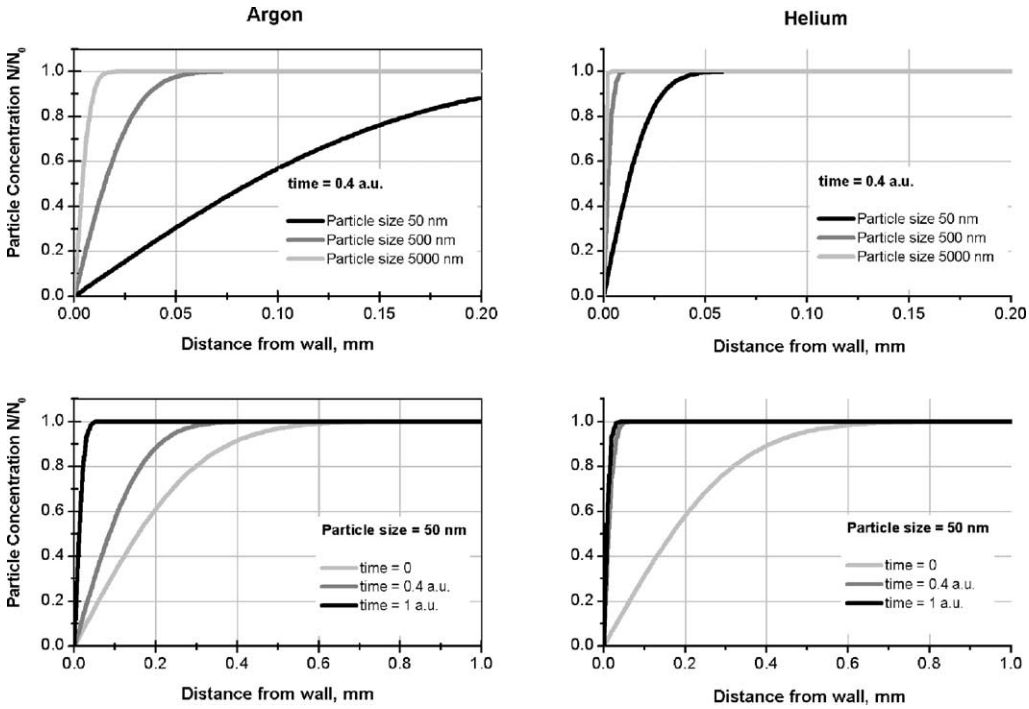

Fig. 8. Calculated particle concentration as a function of wall distance, for different times and particle sizes in argon and helium.

reaction effects. The extent of wall reaction was considered to assess whether it may be a major source of signal deviation for the elements enriching in fine particles. In ablation laser-induced plume assumes spherical symmetry [35,36], which allowed to develop a one-dimensional model of thermophoretic diffusion with hemispherical distribution.

During irradiation, both sample surface and ambient gas are rapidly heated up. Local temperature profile is 'quickly' changing, where how 'quick' depends on ambient gas thermal properties. Due to the gas' thermal diffusivity, the heat dissipation rate and temperature change is more rapid for ablation in He than in Ar. The temperature distribution for the unsteady-state condition was calculated using Fourier's general law of heat conduction [31]. The diffusion coefficient D of a certain particle size was calculated using Stokes–Einstein equation, i.e. $D = kTB$, where k is the Boltzmann constant, T is the temperature and B is a parameter containing the particle diameter, the ambient gas viscosity and the Cunningham slip correction factor [32]. Fig. 7 shows calculated diffusion coefficients for different particle fractions in either Ar or He atmosphere as a function of distance from wall. The diagrams suggest that ablation experiments in Ar lead to wider particle diffusion depth. In Fig. 8 normalized particle concentration as a function of distance from wall in either Ar or He is

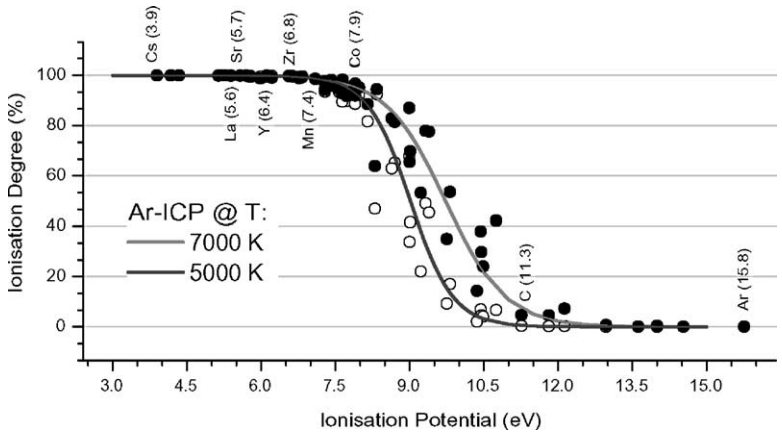

Fig. 9. Ionisation degree of atoms in the argon plasma at different temperatures. The dots are calculated from the atom's and ion's respective partition functions, i.e. black for 7000 K and white for 5000 K (electron number density was $n = 2.82 \times 10^{14}$ and $n = 1.40 \times 10^{12}$ cm^{-3}, respectively). The solid lines are obtained when the partition functions are set equal to one. Polynomial coefficients for the calculation of the partition functions at given temperatures were available from De Galan et al. [29].

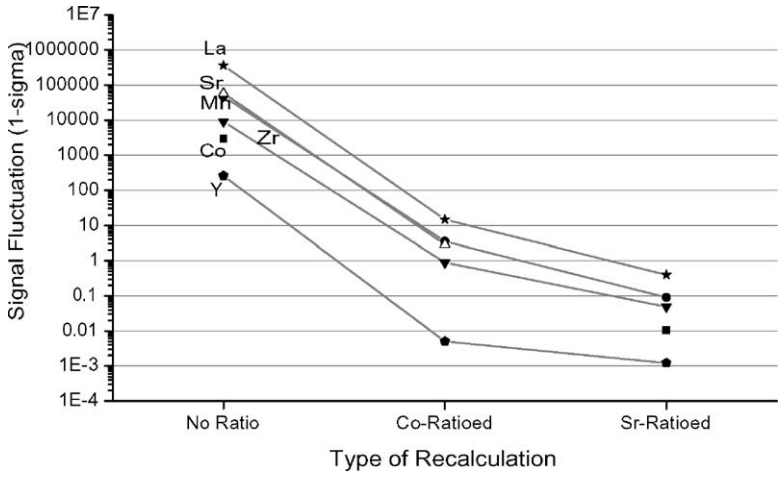

Fig. 10. Average signal fluctuation from sample to sample, as obtained using different data reduction strategies, i.e. with and without internal standardization. Co corrects for plasma temperature fluctuation, whereas Sr corrects for sample delivery fluctuation.

presented for different times and particle sizes, which was derived from Fick's second law of diffusion [32]. Although the curve profiles are qualitatively similar for all particle fractions, quantitatively the wall reaction depth (i.e. the distance from the wall, over which concentration drops from norm values) is wider for Ar at constant particle size, or for fine particles at identical ambient gas. For large particles, the wall reaction depth is practically insignificant in both gases. For nano-size particles in Ar, the interface reaction depth is of the order of magnitude of 1 mm, i.e. almost four-and-half-orders of magnitude larger than the particle size. This permits to conclude that Ar enhances wall reaction compared to He, which might explain the reported [33] 'dirty crater rims' using Ar.

3.3. Sample atomization/ionization

Some workers [24] have maintained that incomplete vaporization of large particles is responsible for fractionation, i.e. inconsistent time-dependent inter-elemental ratios. If the

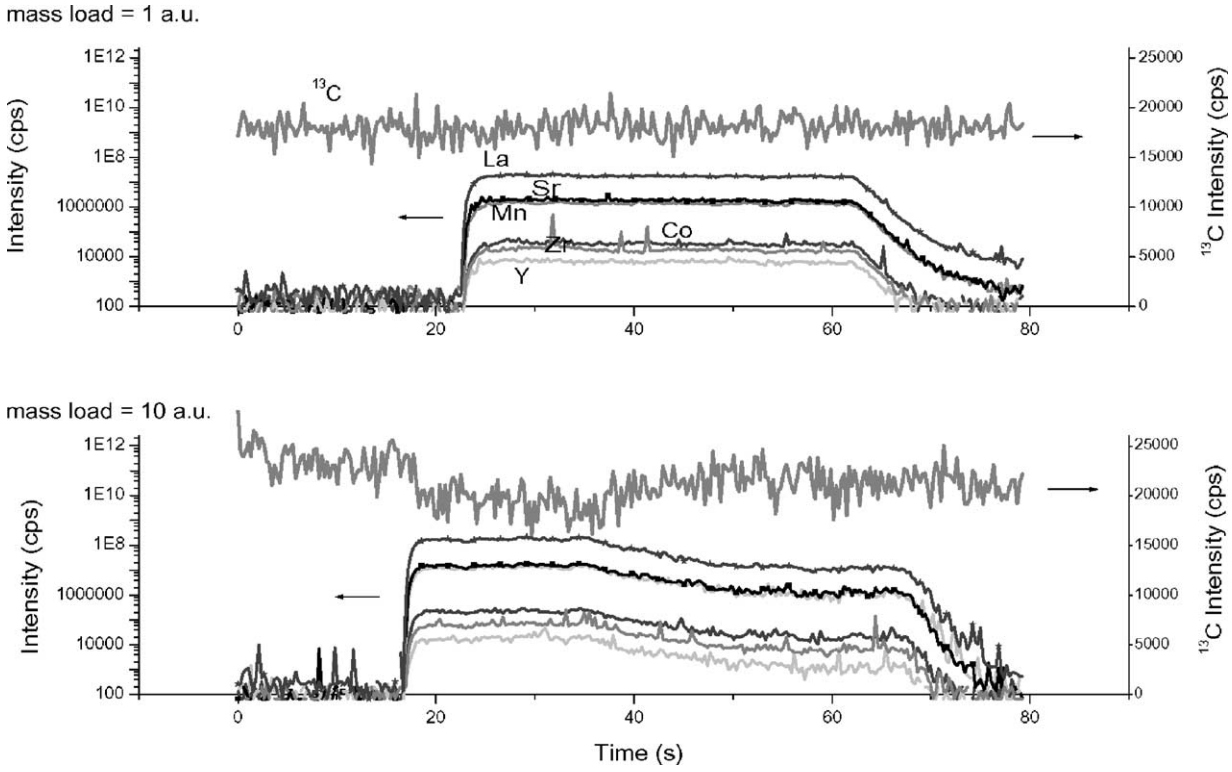

Fig. 11. Signal profile for one-order of magnitude increase in mass load to the ICP. The background shown with ^{13}C signal (right axis).

ICP discharge is responsible for that, this effect should be related with fluctuation in the plasma temperature associated with different mass loads into the ICP. If plasma temperature fluctuates, then atomization/ionization conditions vary, possibly in an element-dependent way. If this qualitative model applies, one should also try to figure out the quantitative extent of it as compared to other sources of signal profile deviation. Fig. 9 shows the calculated ionisation degree as a function of ionisation potential, which is indeed element-dependent. The elements contained in our menu are indicated with ionisation potential in parentheses. Cobalt can be affected as high as 15% in the ionisation degree by temperature fluctuation between 5000 and 7000 K. On the other hand, strontium is virtually independent from plasma temperature fluctuation. Therefore, Co is a good internal standard to correct for ICP temperature fluctuations, whereas Sr is more indicated to correct for fluctuation in the sample delivery. Fig. 10 compares sample to sample fluctuations, using either Co or Sr as internal standard, as well as without internal standard. The plot shows that both sample delivery and ICP fluctuations are responsible for signal profile fluctuation. The former is, however, more significant than plasma temperature fluctuations. Furthermore, when a factor of 10 more mass is introduced into the ICP (Fig. 11), which severely affects the atomization capability (as can be seen from the ^{13}C signal, known that carbon is highly sensitive to temperature fluctuations), the signals of the various elements did track each other anyway. A time-dependent deviation of different elements' signal profiles under high mass load condition could not be produced with the present arrangement by influencing ICP conditions. This might imply that although some particles emerge out of the ICP (incomplete atomization) [30], the portion that has been atomised mostly follows a mechanism of congruent vaporisation, i.e. the vapour that is produced has the same composition of the solid. The exact mechanism of vaporization kinetics is currently under specific investigation and here will not be discussed yet. The figure shows also that some secondary spikes occur specifically for some elements possibly due to clumps.

4. Conclusions

Quantification in LA-ICPMS is still limited by the occurrence of fractionation and availability of reliable standards. The origin of fractionation is still debated and not uniquely attributed. In the present work, it was shown that laser-induced particulate is chemically heterogeneous also using a 266 nm beam. This might lead to non-stoichiometric determinations, if the ablated particulate is not fully transported, atomized, and measured. Particles transport was found to be highly variable as a function of gas regime and particle size. Fluctuations of the sample delivery influence signal profiles in a two-fold way; first, because different sample amounts are being introduced into the ICP-MS over time; second, because mass load effects alter plasma source characteristics. However, it was found that the former of the two factors is typically more remarkable.

The fact that fluctuation in the particle transport alters signal profiles of individual elements matches with previous own observations [28,34], where it was shown that modifying the transport characteristics, by either changing inlet gas flow rate into the sample chamber or trapping the aerosol inside the cell before gating it, isotope-dependent signal enhancement were obtained. Also Guillong and Günther [10] have shown that by filtering a given particle size class, the elemental ratios could be modified, which could further support the idea that different element's signals are 'build-up' by different particle size classes.

Fine particles are efficiently transported, because they transfer into the gas phase as a stable aerosol. Coarse particles are presumably transported by a 'kick-and-bounce' mechanism along the ablation set-up, which renders their delivery not uniform during the ablation duration, which is also suggested by the occurrence of secondary spikes in the transient signal profile.

Therefore, the ablation set-up represents a critical factor in the experimental procedure, especially for depth profile analysis, where signal profile is very important, not simply the integrals.

Acknowledgement

The project ran under EMPA dossier number 840744 in form of post-doctoral fellowship. Th. Graule, P. Holtappels and H.J. Schindler (EMPA) are acknowledged for the samples. U. Gfeller and M. Trottmann (EMPA) are acknowledged for the support during the sample preparation and SEM measurements. D. Bleiner is personally very grateful to Prof. Nimal De Silva (Carleton University, Canada) for the invitation to the ICASS 2003 in Ottawa, where this work has been presented first.

Appendix A

The relationship between the net signal intensity I_{net} and the total (transported) mass m can be expressed as $I = S\,m$, where S is the response factor that is usually experimentally determined via calibration. The mass can be expressed in terms of number of particles N, individual particle volume, and mass density

$$I_{net} = S\,m_{part}\,N = S\,\rho\,V_{part}\,N$$

where m_{part} the mass of a single particle, N the number of particles, ρ is the mass density and V_{part} the volume of the particle. Assuming the particles as spheres, the volume can be calculated from the radius as follows

$$I_{net} = S\,\rho\,\tfrac{4}{3}\pi R^3\,N$$

where R the particle radius. In this equation, all the constants can be grouped in one single control constant. Therefore, an easier expression can be obtained that permits to relate signal intensity and number of transported particles, namely

$$N = \frac{c\, I_{\text{net}}}{R^3}$$

The ratio among different fraction, i.e. relative determination, would permit to cancel out the constant and obtain an estimate of the relative transport efficiency.

References

[1] R.E. Russo, X. Mao, H. Liu, J. Gonzalez, S.S. Mao, Talanta 57 (2002) 425.
[2] J. Gonzalez, X.L. Mao, J. Roy, S.S. Mao, R.E. Russo, J. Anal. At. Spectrom. 17 (2002) 1108.
[3] R.E. Russo, X.L. Mao, O.V. Borisov, Haichen Liu, J. Anal. At. Spectrom. 15 (2000) 1115.
[4] T.E. Jeffries, S.E. Jackson, H.P. Longerich, J. Anal. At. Spectrom. 13 (1998) 935.
[5] M. Montelica-Heino, P. Le Coustumer, O.F.X. Donard, J. Anal. At. Spectrom. 16 (2001) 542.
[6] R.E. Russo, X. Mao, J.J. Gonzalez, S.S. Mao, J. Anal. At. Spectrom. 17 (2002) 1072.
[7] V. Margetic, M. Bolshov, A. Stockhaus, K. Niemax, R. Hergenroeder, J. Anal. At. Spectrom. 16 (2001) 616.
[8] L. St-Onge, J. Anal. At. Spectrom. 17 (2002) 1083.
[9] S.E. Jackson, D. Guenther, J. Anal. At. Spectrom. 18 (2003) 205.
[10] M. Guillong, D. Guenther, J. Anal. At. Spectrom. 17 (2002) 831.
[11] H.P. Jan Kosler, M.N. Longerich, Tubrett, Anal. Bioanal. Chem. 374 (2002) 251.
[12] J. Koch, I. Feldmann, N. Jakubowski, K. Niemax, Spectrochim. Acta, Part B 57 (2002) 975.
[13] O.V. Borisov, X. Mao, R.E. Russo, Spectrochim. Acta, Part B 55 (2000) 1693.
[14] H.R. Kuhn, D. Guenther, Anal. Chem. 75 (2003) 747.
[15] M.E. Taylor, D.L. Blaney, G. Cardell, Appl. Surf. Sci. 165 (2000) 166.
[16] S.M. Eggins, L.P.J. Kinsley, J.M.G. Shelley, Appl. Surf. Sci. 127–129 (1998) 278.
[17] D.J. Figg, J.B. Cross, C. Brink, Appl. Surf. Sci. 127–129 (1998) 287.
[18] P.M. Outridge, W. Doherty, D.C. Gregoire, Spectrochim. Acta, Part B 52 (1997) 2093.
[19] P.M. Outridge, W. Doherty, D.C. Gregoire, Spectrochim. Acta, Part B 51 (1997) 1451.
[20] A.J.G. Mank, P.R.D. Mason, J. Anal. At. Spectrom. 14 (1999) 1143.
[21] H.P. Longerich, D. Guenther, S.E. Jackson, Fresenius J. Anal. Chem. 355 (1996) 538.
[22] J. Koch, A.v. Bohlen, R. Hergenroeder, K. Niemax, J. Anal. At. Spectrom. (2004) 267.
[23] I. Horn, M. Guillong, D. Guenther, Appl. Surf. Sci. 182 (2001) 91.
[24] H.R. Kuhn, M. Guillong, D. Günther, Anal. Bioanal. Chem. 378 (2004) 1069.
[25] P. Richner, D. Evans, At. Spectrosc. 14 (1993) 157.
[26] B. Wanner, C. Moor, P. Richner, R. Broennimann, B. Magyar, Spectrochim. Acta, Part B 54 (1999) 289.
[27] D. Bleiner, GIT Lab. J. 08 (2004) 40.
[28] D. Bleiner, ETH Dissertation, (2002), pp. 14665.
[29] L. De Galan, R. Smith, J.D. Winefordner, Spectrochim. Acta, Part B 23 (1968) 521.
[30] D.B. Aeschliman, S.J. Bajic, D.P. Baldwin, R.S. Houk, J. Anal. At. Spectrom. (2003) 1008.
[31] A.I. Brown, S.M. Marco, Introduction to Heat Transfer, McGraw-Hill, 1951.
[32] P.A. Baron, K. Willeke, Aerosol Measurement: Principles, Techniques, and Applications, second ed., Wiley, 2001.
[33] I. Horn, D. Günther, Appl. Surf. Sci. 207 (2003) 144.
[34] D. Bleiner, D. Günther, in: J.G. Holland, S.D. Tanner (Eds.), Plasma Source Mass Spectrometry: Applications and Emerging Technologies, The RSC Cambridge, 2003, p. 249.
[35] N. Arnold, J. Gruber, J. Heitz, Appl. Phys. A 69 (1999) 87.
[36] M. Hauer, D.J. Funk, Th. Lippert, A. Wokaun, Thin Solid Films 453-454 (2004) 584.